



Structural profiling and biological performance of phospholipid–hyaluronan functionalized single-walled carbon nanotubes

Ram Dvash^{a,c}, Artium Khatchatourians^{b,c}, Leonardo J. Solmesky^d, Peter P. Wibroe^e, Miguel Weil^d, S. Moein Moghimi^e, Dan Peer^{a,c,*}

^a Laboratory of NanoMedicine, Dept. of Cell Research & Immunology, George S. Wise Faculty of Life Sciences, Tel Aviv University, Tel Aviv 69978, Israel

^b Laboratory of Bio-AFM, Tel Aviv University, Tel Aviv 69978, Israel

^c Center for Nanoscience and Nanotechnology, Tel Aviv University, Tel Aviv 69978, Israel

^d Cell Screening Facility for Personalized Medicine, Laboratory for Neurodegenerative Diseases and Personalized Medicine, Department of Cell Research and Immunology, George S Wise Faculty of Life Sciences, Tel Aviv University, Tel Aviv 69978, Israel

^e Nanomedicine Research Group, Centre for Pharmaceutical Nanotechnology and Nanotoxicology, and NanoScience Centre, University of Copenhagen, DK-2100 Copenhagen, Denmark

ARTICLE INFO

Article history:

Received 18 February 2013

Accepted 29 May 2013

Available online 10 June 2013

Keywords:

Carbon nanotubes

Hyaluronan

Immune response

Cytotoxicity

High-content analysis

ABSTRACT

In spite of significant insolubility and toxicity, carbon nanotubes (CNTs) erupt into the biomedical research, and create an increasing interest in the field of nanomedicine. Single-walled CNTs (SWCNTs) are highly hydrophobic and have been shown to be toxic while systemically administrated. Thus, SWCNTs have to be functionalized to render water solubility and biocompatibility. Herein, we introduce a method for functionalizing SWCNT using phospholipids (PL) conjugated to hyaluronan (HA), a hydrophilic glycosaminoglycan, with known receptors on many types of cancer and immune cells. This functionalization allowed for CNT solubilization, endowed the particles with stealth properties evading the immune system, and reduced immune and mitochondrial toxicity both *in vitro* and *in vivo*. The CNT–PL–HA internalized into macrophages and showed low cytotoxicity. In addition, CNT–PL–HA did not induce an inflammatory response in macrophages as evidenced by the cytokine profiling and the use of image-based high-content analysis approach in contrast to non-modified CNTs. In addition, systemic administration of CNT–PL–HA into healthy C57BL/6 mice did not alter the total number of leukocytes nor increased liver enzyme release as opposed to CNTs. Taken together, these results suggest an immune protective mechanism by the PL–HA coating that could provide future therapeutic benefit.

© 2013 Elsevier B.V. All rights reserved.

1. Introduction

Due to their outstanding properties, carbon nanotubes (CNTs) have emerged as promising nanomaterials in nanomedicine as both drug delivery vehicles and diagnostic tools [1–5]. The great interest in CNTs for biomedical applications derives from their unique structure and properties, which can be potentially exploited in a broad range of biomedical applications. CNTs have intense and unique Raman scattering, enabling easy detection in a variety of environments [6]. Their high aspect ratio enables to enhance the specificity and/or the potency of the particles by binding more biological species per particles [7]. Due to their hydrophobic nature, insoluble chemotherapeutic agents [8] and some proteins [9] adsorb spontaneously to CNT's sidewall and enable binding of functional groups. CNTs

have been shown to cross the cell membrane in mammalian cells [10], and therefore have been used as transfection reagents in delivering nucleic acids such as small interfering RNAs (siRNAs) into a broad range of cells [11,12]. Many biological applications using CNTs have emerged in recent years. CNTs were used as protein carriers in transporting cytochrome c and its functionality was demonstrated by induction of cell apoptosis [9]. In another study, enhanced tumor suppression in mice was shown. The chemotherapy Paclitaxel was conjugated to polyethylene glycol functionalized CNTs and used to treat breast cancer in a murine model. The particles have enhanced efficacy in comparison with commercial Paclitaxel formulation (Taxol) [13].

Short SWCNTs (less than 100 nm) were used as non-viral vectors for the delivery of oligonucleotides (synthetic oligonucleotides containing the DNA binding sequence of a transcription factor) against nuclear factor- κ B (NF κ B) to human macrophages [14]. Together with the efforts of using CNTs as drug delivery vehicles, there were also attempts to use CNTs as imaging agents. The chelate DOTA was attached covalently to CNTs and was loaded with ¹¹¹In

* Corresponding author at: Laboratory of NanoMedicine, Dept. of Cell Research & Immunology, George S. Wise Faculty of Life Sciences, Tel Aviv University, Tel Aviv 69978, Israel.

E-mail address: peer@tauex.tau.ac.il (D. Peer).

for radiolabeling. Rituximab monoclonal antibody (against CD20 expressed on B cells and up-regulated in many types of lymphoma and leukemia) was also attached to CNTs, and thus, a target specific contrast agent was constructed [15]. To exploit all unique properties of CNTs, their hollow tube was filled with metal halides that were used as radioprobes (tracked with single photon emission computed tomography) [16]. The primary and most critical step when trying to harness CNTs into biomedical applications is to overcome their insolubility in aqueous solutions such as water, buffers, growth media and sera. This poor-water solubility represents the main hurdle in utilizing CNTs in biomedical applications. Moreover, pristine CNTs were shown to have toxic effects when applied *in vitro* and *in vivo*. But it was also shown that properly functionalized CNTs have reduced toxic effects [17]. Two approaches for functionalization are employed for CNT modification: covalent and non-covalent. The benefit derived from non-covalent functionalization is that it does not interrupt the atomic lattice, and hence, the electronic properties of the tubes remain intact, whereas the benefit of the covalent method allows stable functionalization. In this respect, covalently functionalized SWCNTs exhibit reduced Raman absorption cross-sections [18]. In order to solubilize CNTs, various methods were developed to non-covalently functionalize CNTs including the use of surfactants, polymers, nucleic acids, peptides and proteins. In principle, all methods add soluble groups to the backbone of the CNTs and thus facilitate solubility. The attachment of relatively large functional groups is required to solubilize CNTs. Herein, we devised a strategy that utilized hyaluronan (HA) with its outstanding solubility characteristics as well as biocompatibility, as the functionalization agent on the surface of SWCNTs. HA, composed of repeating disaccharide units of D-glucuronic acid and D-N-acetylglucosamine linked *via* alternating β -1,4 and β -1,3 glycosidic bonds, is a high molecular weight glycosaminoglycan, and it is ubiquitously present in the extracellular matrix. It has many biological roles, including maintaining the extra cellular matrix (ECM) architecture and water retention, cell motility, migration and proliferation regulation, and cell adhesion and activation, and in tumor metastasis [19,20].

In this study, CNTs were conjugated to HA using phospholipids as the linking arm between HA and CNT. These particles have very good stability in aqueous solutions as reinforced by their zeta potential analysis. The effect of the structure of the phospholipid's hydrophobic tail on its ability to disperse CNTs was evaluated. Particle structure was analyzed by scanning electron microscopy (SEM) and by transmission electron microscopy (TEM). To confirm that these new nanotubes can be used in biological settings, their toxicity *in vitro* and *in vivo* was assessed using proliferation assays, high-content analysis and cytokine induction profile in cell lines along with measuring complement activation in human sera, leukocyte counts and liver enzyme release in healthy mice during a single and multiple intravenous administrations.

2. Materials and methods

2.1. Conjugation of phospholipids to hyaluronan

The carboxyl groups of HA and the primary amines of the phospholipids (phosphatidylethanolamine; PE) were exploited for conjugation. Using amine-coupling chemistry these two molecules were cross-linked. HA (750,000 kDa, Lifecore Biomedical, LLC (MN, USA)) was dissolved in doubled distilled water (DDW) to a final concentration of 5 mg/ml (HA solution). DPPE (Avanti Polar Lipids, Alabaster, AL, USA) was dissolved in ethanol (96%) at 1 mg/ml at 60 °C (DPPE solution). HA solution was activated for 15 min with carbodiimide (EDAC, 0.2 M) and sulfo-N-hydroxysuccinimide (NHS, 0.3 M) both purchased from Sigma-Aldrich Co. (St. Louis, MO, USA) at room temperature. Activated HA solution and DPPE solution were mixed at 1:1 ratio (v/v) and incubated for 2 h at 60 °C. The liquid was evaporated

completely to discard the ethanol and the remnant was resuspended in DDW (equal volume). The aqueous solution was centrifuged at 300,000 g for 1 h and these washings were repeated three additional times to remove large HA aggregates.

2.2. Self-assembled CNT-PL-HA

1 mg of pristine CNTs (pCNT) (S-Purified Single-walled Nanotubes) as well as carboxylated carbon nanotubes (CNT-COOH), 50–70% carbon basis, D \times L 1.2–1.5 nm \times 2–5 μ m, bundle dimensions were purchased from Sigma-Aldrich (St. Louis, USA).

pCNTs were suspended in 1 ml of the PL-HA solution as detailed above and sonicated in an ultrasonic water bath (Cole-Parmer, 100 W, 42 kHz) for 1 h. The solution was then washed three times to remove aggregates (10 min, 5000 g). To remove the excess HA-PL, the CNT suspension was centrifuged at 200,000 g for 45 min and the pellet was recovered. The final washing step was repeated and the pellet was suspended in DIW or PBS or any desired media (at this stage the concentration of the final solution could be determined) by spectral analysis in 808 nm. The suspension was sonicated again for 1 h and washed once (10 min, 5000 g) to remove non-dispersed material.

2.3. Phospholipids and quantitative analysis

Three different phospholipids (DOPE, DLPE and DPPE), all purchased from Avanti Polar Lipids Inc. (Alabaster, AL, USA) were covalently attached to HA to assess their ability to disperse SWCNT. All PL-HA conjugates were prepared as described and the absorbance at 808 nm (Cary-5000) of the suspensions (CNT-PL-HA) was measured to determine CNT concentration. Phospholipids were assayed by the lipid mass, modified Bartlett assay as previously described [21–23].

2.4. CNT structure analysis by electron microscopy

High-resolution Scanning Electron Microscopy (HRSEM-JEOL JSM-6700) and Transmission Electron Microscopy – TEM (JEOL 1200EX) were used for morphological assessment of the carbon nanotubes. Pristine CNTs were suspended in 1% Tween 80 solution, whereas the PL-HA counterparts were suspended in PBS. For HR-SEM, samples (0.1 mg/ml) were air dried on a silicon wafer and coated using a chrome sputter. For TEM, samples (0.1 mg/ml) were stained with uranyl acetate (2% in water) on a carbon-coated copper grid.

2.5. CNT structure analysis by Atomic Force Microscopy

AFM imaging and analysis was performed on a JPK NanoWizard III AFM system (JPK Instruments AG, Berlin, Germany), with tip scanning. Intermediate contact (tapping) mode was used. The AFM probe used was that of MicroMasch, NSC15/AIBS – a quite rigid, standard tapping mode probe, made of silicon, with Al coating on the cantilever backside. The resonance frequency was around 300 kHz and the line rate used was 0.5 Hz to 1 Hz, and 512 \times 512 pixels.

Samples were prepared by placing a drop of stock solution of either pCNTs or CNT-PL-HA compounds on a freshly cleaved mica substrate.

2.6. Zeta potential measurements

The electrophoretic mobility of carbon nanotubes was measured using a Malvern ZetaSizer Nano ZS instrument at pH 6.7, 20 °C, with 10 mM NaCl. Each experimental result is the average of six independent measurements. CNT concentration of all the samples was 10 μ g/ml.

2.7. Cell proliferation assay

To evaluate the effect of CNT–PL–HA on cell proliferation, XTT (sodium 2,3-bis(2-methoxy-4-nitro-5-sulfophenyl)-5-[(phenylamino)-carbonyl]-2H-tetrazolium) assay was employed. Murine macrophages (RAW 264.7) and the epithelial colon adenocarcinoma cells (HCT 116) were used as model cells for leukocytes and epithelial cells. RAW 264.7 or HCT 116 0.2×10^6 cells/well (in a 96-well plate) were incubated with the nanotubes at three different carbon concentrations (4.8, 9.09 and 16.67 $\mu\text{g}/\text{ml}$) and the assay was performed at 24, 48 and 72 h post nanotube addition.

2.8. Internalization analysis of CNT–PL–HA and CNT into macrophages using confocal microscopy

Internalization assay was performed in 24 well plates. 2.0×10^6 RAW 264.7 were seeded on cover slips in DMEM medium, supplemented with antibiotics, L-glutamine and 10% fetal calf serum (Biological Industries, Beit Haemek, Israel).

For nuclei staining, cells were stained with Hoechst (2.5 mg/ml stock, 1:10,000 in PBS) (33258, Sigma). For CNT labeling, Lissamine™ rhodamine B-1,2-dihexadecanoyl-sn-glycero-3-phosphoethanolamine, triethylammonium salt (rhodamine DHPE) (L-1392, Invitrogen) was added during the particle preparation for CNT–PL–HA and water soluble rhodamine conjugated dye (Life Technologies, Carlsbad, CA, USA) was directly conjugated to CNT–COOH using amine coupling technique as previously reported [24]. Concanavalin A-Alexa488 (1.5 $\mu\text{g}/\text{ml}$) was used for staining the membrane (Sigma), and Deep Red labeled MitoTracker™ (Invitrogen) was used for selective probing of cell mitochondria. The cells were exposed (10 μg CNT or CNT–PL–HA, 50 μl from the prepared nanotube stock solution) to medium without serum for a period of 20 min at 37 °C in a humidified atmosphere with 5% CO₂. Subsequently, the cells were washed twice using cold PBS \times 1, pH 7.4, fixated with 4% paraformaldehyde (PFA) and washed again with cold PBS. Membrane and nuclei staining were performed after fixation. The cells were mounted on a fluorescent mounting medium (Golden Bridge International, Mukilteo, WA, USA) and fluorescence was measured using an Andor Spinning Disk Confocal Microscope and a Meta 510 Zeiss LSM Confocal Microscope. Serial optical sections of the cells were recorded for each treatment and the images were processed using Zeiss LSM Image browser software.

2.9. Image-based high content analysis (HCA)

Image-based high content analysis (HCA) is an advanced fluorescent microscopy that allows for concomitant quantification of probe/reporter signal intensities, and measurement of cell and sub-cellular morphology parameters. Thus, this technology produces a multi-parametric output based only on cell images that allow quantification and profiling of different phenotypes. To gain insight into a broader biological understanding of the effect of both pCNT and CNT–PL–HA we decided to study their effect on macrophages in culture by means of HCA. To achieve this goal we cultured macrophages (0.2×10^6 cells/well in a 96 well-plate) in the presence of 16.67 $\mu\text{g}/\text{ml}$ of either pCNT or CNT–PL–HA. Cells without CNTs served as control. Following 24, 48 or 72 h of culture, the cells were washed with PBS \times 1, pH 7.4 and the cells were cultured for an additional 8 h in medium without any CNT to allow cell recovery. The cells were stained for 30 min at 37 °C with Hoechst 33342 (Sigma) (for visualizing the nuclei), Calcein AM (Invitrogen) (for selective staining of live cell cytoplasm), propidium iodide (Sigma) (for specific visualization of dead cell nuclei) and Deep Red labeled MitoTracker™ (Invitrogen) (for selective probing of cell mitochondria). The stained cells were subjected to image acquisition employing the IN Cell Analyzer 2000 (GE Healthcare) and the obtained images were analyzed employing the imaging system manufacturer software. In order to analyze the figures,

each channel was segmented employing algorithms based on the iterative comparison of levels of grays in each pixel and their neighbors (kernel and sensitivity of object segmentation were established by the user according to iterative analysis–validation cycles). The resulting bitmaps were linked to produce combined segmented bitmaps allowing the measurement of each sub-cellular stained structure morphological parameters within each cell.

2.10. Cytokine production assay

The effect of CNT–PL–HA on the induction of the cytokines TNF- α and IL-10 was performed on the macrophage cell-line RAW 264.7 Cells (0.2×10^6 cells/well) were seeded in DMEM with 10% v/v FBS and incubated (37 °C, 5% CO₂) 48 h before nanotube addition. After the addition of the CNTs, cells were incubated for 4 or 24 h and supernatants from the cell cultures were obtained and stored at –80 °C until further use.

To detect cytokine expression an ELISA for detecting TNF- α and IL-10 was carried according to the manufacturer's instructions, R&D Systems (Minneapolis, MN, USA).

2.11. Complement activation studies

Details for human serum preparation, characterization and functional assessment of complement pathways were in accordance with our previous studies [25,26]. To measure complement activation *in vitro*, we determined CNT-induced rise of serum complement activation products SC5b-9 using Quidel ELISA kits (Quidel, San Diego) according to the manufacturer's protocols as described previously [25]. For measurement of complement activation, the reaction was initiated by adding the required quantity of nanotubes to undiluted serum in Eppendorf tubes in a shaking water bath at 37 °C for 30 min. Reactions were terminated by addition of sample-diluent provided in the assay kit containing 25 mM EDTA. CNT-induced rises of serum complement activation products were then measured following nanotube removal by centrifugation. Control serum incubations contained saline (the same volume as nanotubes and other additions) for assessing background levels of complement activation products. Zymosan (1 mg/ml) was used as a positive control for complement activation throughout. For quantification of complement activation products, a standard curve was constructed using the assigned concentration of standards supplied by the manufacturer and validated. The slope, intercept and correlation coefficient of the derived best-fit line for SC5b-9 standard curve were within the manufacturer's specified range. The efficacy of CNT treatments was established by comparison with baseline levels using paired t-test; correlations between two variables were analyzed by linear regression, and differences between groups (when necessary) were examined using ANOVA followed by multiple comparisons with Student–Newman–Keuls test.

2.12. Animal care and treatment

Animals, healthy C57BL/6 mice, ~20 g/mouse, 9 weeks old, were obtained from the animal-breeding center, Tel-Aviv University (Tel Aviv, Israel). Animals were maintained and treated according to the National Institutes of Health guidelines. All animal protocols were approved by the Tel-Aviv Institutional Animal Care and Use Committee.

2.13. Blood biomarker assays

To assess blood biomarkers such as total leukocyte number, liver enzyme release and cholesterol level, pCNT (Tween 80 dissolved in DIW (0.125% v/v)) and CNT–PL–HA were prepared and intravenously injected into the tail vein of C57BL/6 (8 weeks old) mice, 100 μl at 1 mg/kg ($n = 6$ mice/group). 2, 6 and 24 h post i.v. injections and

an additional experiment at day 0, 2, and 4 from experiment initiation (at the same dose, $n = 5$ mice/group) were performed. 24 h post the last injection, blood was drawn and the serum was obtained by centrifugation of the whole blood at 850 g for 15 min in a protocol we previously reported [22] and was applied into a COBAS MIRA auto analyzer (Roche) to analyze the levels of liver enzymes Alanine Amino-transferase (ALT) and Aspartate Aminotransferase (AST), as well as cholesterol levels and the number of major groups of leukocytes.

2.14. Statistical analysis

In vitro data were analyzed using unpaired Student's t-test. Differences between treatment groups were evaluated by one-way ANOVA with significance determined by Bonferroni adjusted t-tests.

3. Results and discussion

3.1. Preparation of PL-HA coated single-walled nanotubes

CNTs have recently emerged as promising nanomaterials for imaging and drug delivery applications [19,27–29]. The two primary hurdles, which need to be addressed in order to utilize CNTs for bio-applications are their insolubility in aqueous solutions and their toxicity. Here, we present a new approach to functionalize CNTs for biological applications with high water solubility and low toxicity. The ability of PL-HA complex to solubilize CNTs can reach up to 1 mg/ml. The alkyl chains of the phospholipids interact with the

aromatic rings on the sidewall of the CNTs. The hydrophilic hyaluronan that bonded covalently to the phospholipid dissolves in the aqueous solution and disperse the suspension (Fig. 1).

In order to attach the charged polysaccharide HA to the graphene backbone of pristine SWCNTs (pSWCNTs), a mediator is required. Phospholipid molecules with a primary amine group (phosphatidyl-ethanolamine) have a hydrophobic chain (diglyceride) and a primary amine group that can be chemically exploited. 1,2-Dipalmitoyl-sn-glycero-3-phosphoethanolamine (DPPE) was conjugated to HA to create an amphiphilic molecule (PL-HA). We have previously characterized this conjugate by different analytical methods as reported [30] detecting both the lipids and HA. CNTs were added to a solution containing PL-HA suspension as detailed in the experimental section and were sonicated to create the aqueous suspension (Fig. 1a). In a control experiment, with identical materials lacking the crosslinkers, the CNTs could not be dispersed in the solution (Fig. 1b).

To explore the effect of different PE structures on the particle formation, and to estimate which PE side chain has a better capability in facilitating CNT-PL-HA nanotube formation, three different types of PE were examined: 1,2-dioleoyl-sn-glycero-3-phosphoethanolamine (DOPE), 1,2-dipalmitoyl-sn-glycero-3-phosphoethanolamine (DPPE) and 1,2-dilauroyl-sn-glycero-3-phosphoethanolamine (DLPE). DOPE was inferior in its ability to create and disperse nanotubes in comparison with DPPE and DLPE (data not shown). We did not observe substantial differences between the DPPE and DLPE in dispersing the generated CNTs, indicating that the difference in the carbon side chain is not a major factor for dispersing the CNTs. Analytical

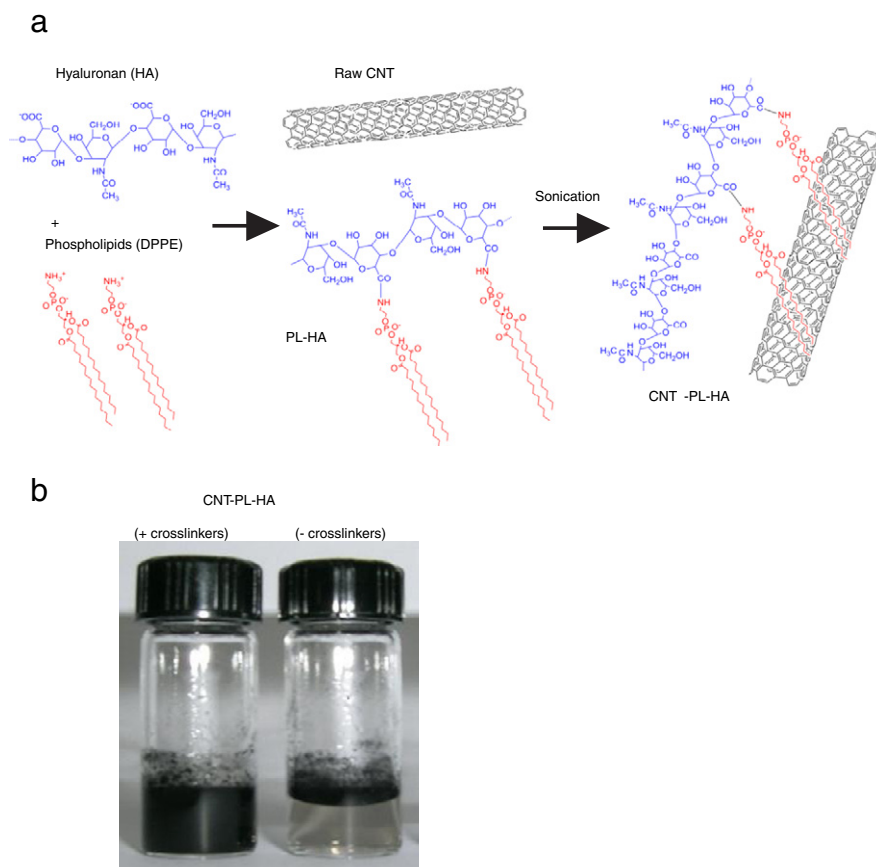


Fig. 1. Dispersing CNT using PL-HA conjugates. (a) A schematic illustration of CNT-PL-HA particle production chemistry: First, hyaluronan molecules were conjugated to 1,2-dipalmitoyl-sn-glycero-3-phosphoethanolamine (DPPE) with zero-length crosslinkers creating the amphiphilic molecule, PL-HA. Second, pristine SWCNT were added to the PL-HA solution and the resulting CNT-PL-HA was sonicated in a bath sonicator creating an aqueous suspension of CNT-PL-HA particles. (b) To each vial, 1 mg of pristine SWCNTs were added and the solutions were sonicated for 1 h. Left vial: HA and DPPE conjugated with crosslinkers, a homogenous solution was formed. Right vial: HA and DPPE solution without crosslinkers (same procedures were taken on both solutions), no two-phase solution was formed.

measurements of the amounts of phospholipids were performed as previously described [21] confirming the presence of the phospholipids on CNTs.

3.2. Structural and physicochemical characterization of CNT-PL-HA

We next examined CNTs under scanning electron microscopy (SEM) and transmission electron microscopy (TEM). When comparing the SEM images of pSWCNTs (Fig. 2a) and CNT-PL-HA particles (Fig. 2b), we observed that pSWCNTs tend to aggregate, while CNT-PL-HA particles seem to be dispersed equally in the solution (Fig. 2b) with no aggregations.

In order to utilize TEM analysis, samples were stained with uranyl acetate. A drop of solution was stained with uranyl acetate and then dried on a carbon coated copper grid. The major difference between pSWCNTs (Fig. 3a) and PL-HA coated CNTs (Fig. 3b) was the dark shading surrounding the latter nanotubes. We speculate that these shadows mark the presence of the HA since uranyl acetate is positively charged and is known to bound to the negatively charged HA [31,32].

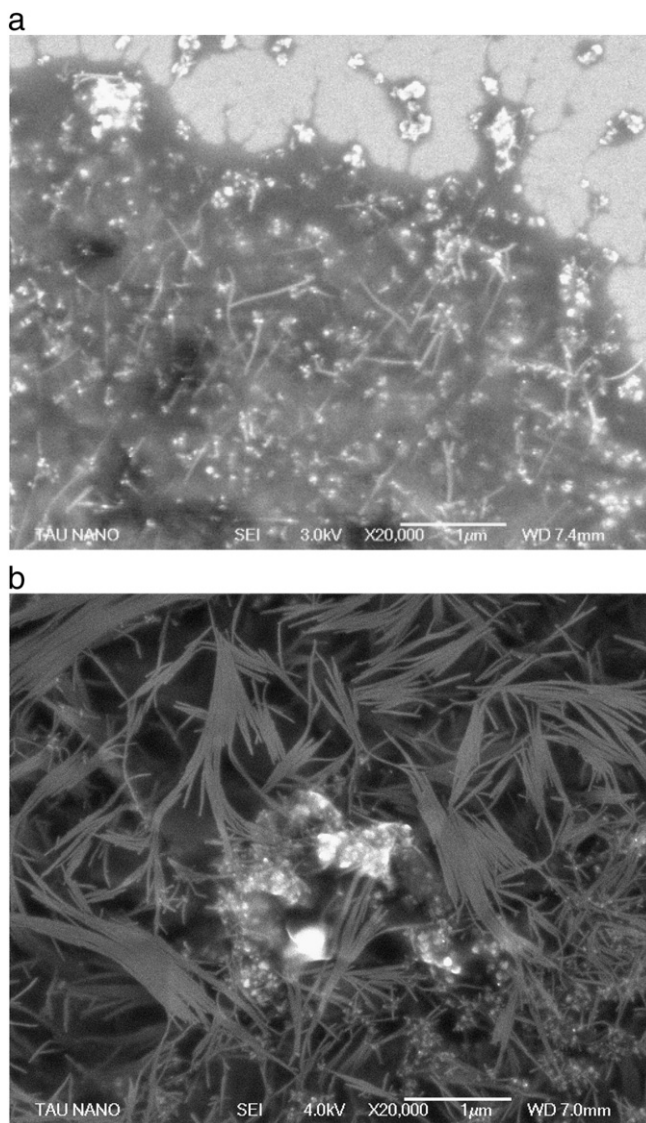


Fig. 2. Surface images of pSWCNT and CNT-PL-HA using HR-SEM. (a) Representative images of equally dispersed CNT-PL-HA nanotubes when dissolved in aqueous solution. (b) Representative images of aggregate bundles of pSWCNT observed after dissolving in aqueous solution by a detergent.

We also performed an AFM analysis, and deposited the pCNT or CNT-PL-HA on freshly cleaved mica (Fig. 4). When deposited, a relatively low concentration of pCNTs and some small CNT aggregates could be observed, from them it was possible to see fragments of separate CNTs (data not shown). For higher concentrations, the pCNTs were “embedded” in some very large (relatively) conglomerates of unknown material. This made the estimation of their height very difficult or nearly impossible.

For CNT-HA compounds, again, the CNTs could be in principle observed, but they look “embedded” and “sunk” in a matrix of some other material, probably the CNT-HA aggregates themselves, that form the morphology of surface roughness of tens of nanometers on the mica surface.

When deposited, CNT-PL-HA on the mica at a higher concentration, the CNTs could be in principle observed, but they look “embedded” and “sunk” in a matrix of some other material, probably the CNT-PL-HA aggregates themselves, that form the morphology of surface roughness of tens of nanometers on the mica surface.

So, we had to figure out the characteristic dimensional properties of the CNTs using “non-direct” methods.

One of them is phase imaging. In phase imaging, the feature edges are usually observed as being sharper, and also phase imaging allows visualizing features of different height ranges at the same contrast level, which is quite difficult or impossible in topography images. Phase images provide the opportunity to assess the CNT length and width. Taking into account that the CNTs are cylindrical in shape, we can thus estimate their height/diameter as well. The height estimation can be still further confirmed in line profile measurements of topography images, even though the contrast for low height features on them is not optimal.

From the phase image of pCNTs (Fig. 4a) and CNT-PL-HA (Fig. 4b) one can derive the characteristic CNT length, which is in the range of 1.5–2 μm , and their characteristic width, which is actually their diameter. The line profile measurements of the lateral CNT width revealed the value of about 25–30 nm, which is in the order of magnitude of the AFM tip itself. Thus, the observed CNTs are single-walled, so, their diameter should be in the range of 1–2 nm. This was also supported by the height measurements of the separate CNTs on a spot obtained from suspension of low CNT concentration. The obtained height then was about 2 nm.

Thus, the aspect ratio (length to diameter ratio) of the CNTs is estimated to be about 1000, which falls in the range of the reported dimension from the data sheet provided for the raw pCNT.

Another line of investigation that might confirm the presence of HA on the surface of the CNTs is the measurements of nanotube electrophoretic mobility.

The zeta potential of CNT-PL-HA in DIW was $-42.9 \text{ mV} \pm 2.7 \text{ mV}$, whereas pCNTs had a zeta potential of $-14.7 \pm 2.2 \text{ mV}$.

3.3. CNT-PL-HA do not exhibit cytotoxic effects on macrophages and epithelial cells

Cytotoxicity may set a substantial limitation when harnessing CNTs in biological settings. To evaluate the cytotoxicity of CNT-PL-HA, proliferation assays on two different cell lines representing macrophages (RAW 264.7) and epithelial (HCT 116) cells were performed. When probing the effect of CNT-PL-HA on macrophages, it appears that no substantial changes in cell proliferation are observed at three concentrations, ranging from 4.8, 9.1 and up to 16.7 $\mu\text{g/ml}$ when these nanotubes are cultured for 72 h, in contrast to pristine CNTs, which had a significant effect on cell proliferation in a dose dependent manner (Fig. 5a). The same trend was observed when human colon adenocarcinoma cells were used (Fig. 5b). This effect seems to be derived from the presence of CNTs and not affected by the presence of the solvent itself since the same concentration of the solvent was tested and was not effecting cell proliferation.

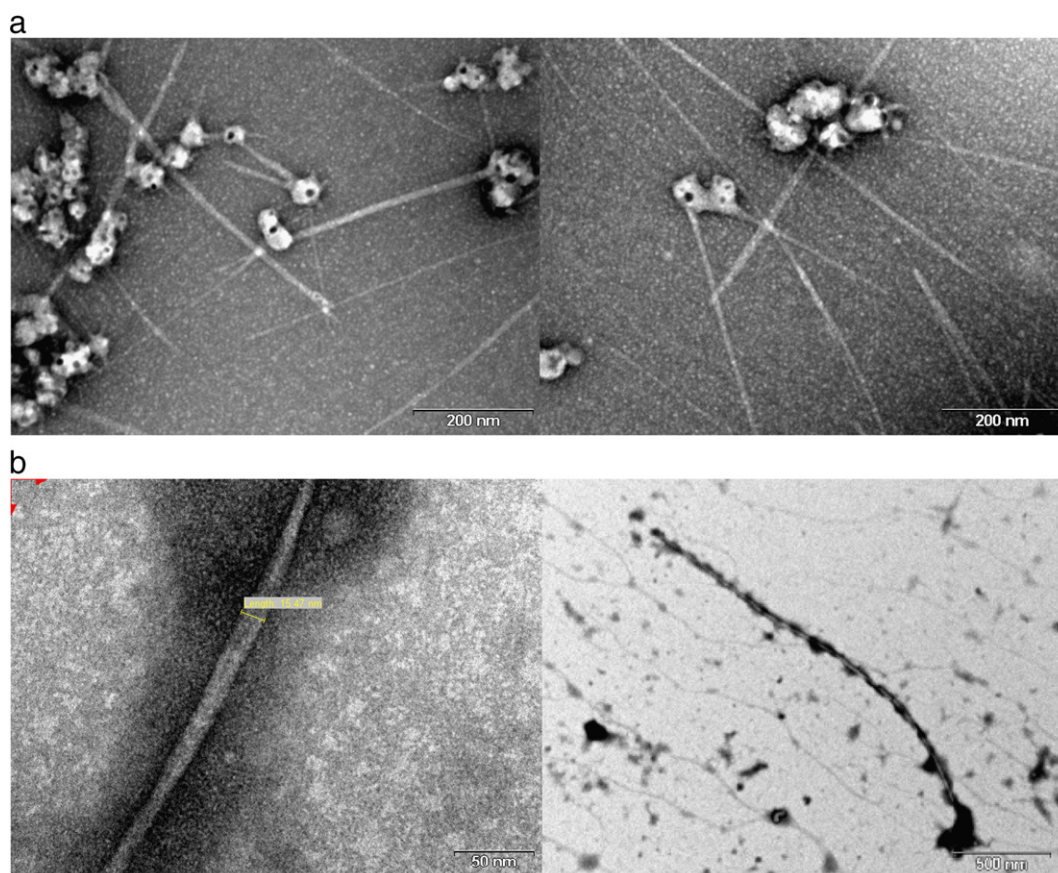


Fig. 3. TEM analysis of pSWCNT and CNT-PL-HA particles. (a) Representative images of pSWCNTs. (b) Representative images of CNT-PL-HA particles. The samples were stained with uranyl acetate prior to use. As opposed to pSWCNTs (a), the backbone of CNT-PL-HA particles is surrounded with dark shadowing supporting the presence of HA. Images were taken from at least three independent preparations with minimal batch-to-batch variations.

3.4. CNT-PL-HA and CNT are taken up by macrophages

In order to investigate the potential cytotoxic effect observed with the CNT and the minimal toxicity observed with the CNT-PL-HA, we examined the internalization of these nanotubes into murine macrophages using confocal microscopy. Surprisingly, we did not find any different patterns in the internalization process of both nanotubes since both of them internalized into macrophages within 20 min of incubation (Fig. 6). However, it is highly possible that the mechanism of internalization is different and therefore, the intracellular trafficking could be different.

To try and reveal the mechanism of this cytotoxicity of CNTs in macrophages, we utilized an image-based high content analysis approach [33].

3.5. Image-based high content analysis reveals mitochondrial toxicity of pristine CNTs but not of CNT-PL-HA

High-content analysis (HCA) technology produces a multi-parametric output based only on cell images, which allows quantification and profiling of different phenotypes.

We have previously used this approach to reveal new types of cytotoxic effects derived by lipid-based nanoparticles on human fibroblasts [33], where we have found a direct connection between the use of HCA technology examining mitochondrial toxicity caused by cationic lipids and ROS. In this study, we observed decrease in cell viability (using the XTT assay) when applying pCNTs. We thought to examine mitochondrial morphological changes using HCA since XTT measures mitochondrial enzyme. As detailed in the experimental section, we cultured macrophages in the presence of 16.67 $\mu\text{g/ml}$ of

either CNT or CNT-PL-HA. Cells without CNTs served as control. 24, 48 or 72 h post culture, cells were washed with PBS \times 1, pH 7.4 and were further cultured for an additional 8 h without any CNT addition, to allow for cell recovery, then stained as detailed in the [Materials and methods](#) section. The stained cells were subjected to image acquisition employing the IN Cell Analyzer 2000 (GE Healthcare) and the obtained images were analyzed using the imaging system manufacturer software. Among the various HCA variables we decided to focus on the mitochondrial activity in the cells.

Fig. 6 represents the mitochondrial activity in the macrophages upon treatment with CNTs or CNT-PL-HA.

Mitochondrial total area (Fig. 7a) – represents the total area of mitochondrial inclusions attributed to the cell. This parameter gives an indication of general mitochondrial activity. *Mitochondrial count* (Fig. 7b) – represents the actual number of inclusions stained by MitoTracker™ attributed to the cell. It reflects mitochondrial activity and mitochondrial aggregation, which is related to cytotoxic effects. *Mitochondrial mean area* (Fig. 7c) – mean area of mitochondrial inclusions (averaged by all inclusions within the cell). This parameter gives an indication of mitochondrial activity and aggregation and could be affected by a toxic response. *Mitochondrial mean intensity* (Fig. 7d) – average intensity of pixels within mitochondrial inclusions. This gives an indication of mitochondrial activity.

Macrophages treated for 72 h, but not for a shorter period of time, with CNTs showed a significant difference in mitochondrial parameters (Fig. 7) compared with mock-treated cells and with CNT-PL-HA-treated cells, indicating that the treatment with CNT maybe reflecting mitochondrial damage and this process takes about 72 h. Overall, these results clearly suggest that CNT is toxic to macrophages and its toxicity is directly related to the mitochondrial activity, CNT-

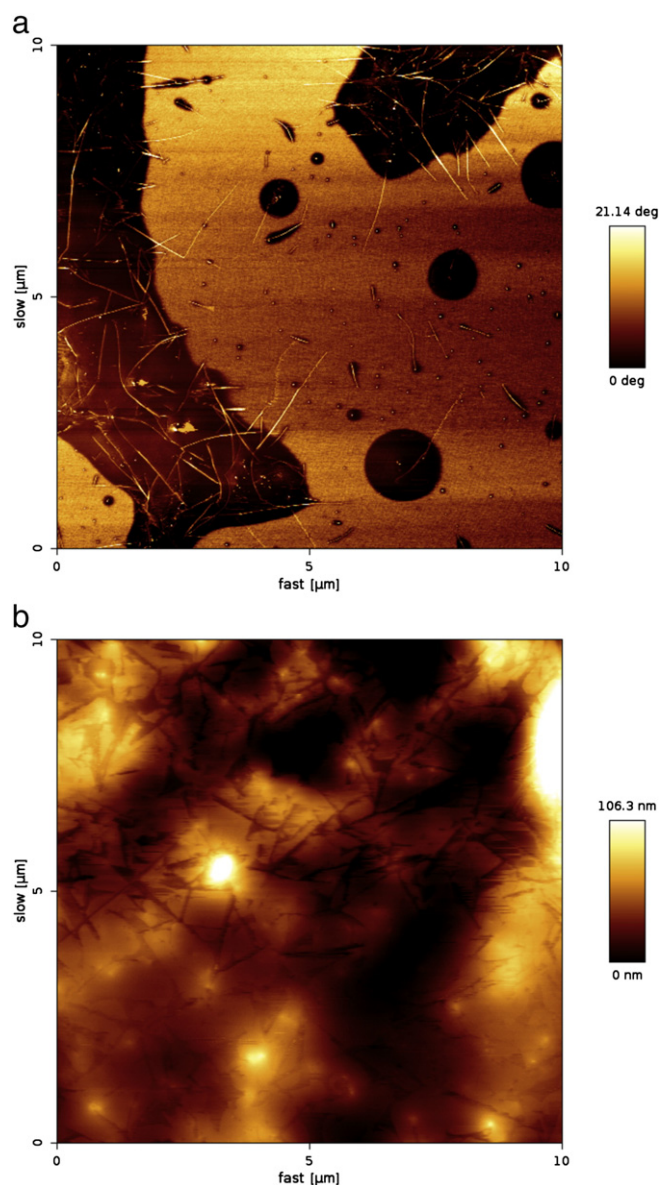


Fig. 4. AFM analysis of pCNT and CNT-PL-HA. Representative phase AFM image of pCNTs deposited on mica substrate. (b) Representative topography (height) AFM image of CNT-PL-HA deposited on mica substrate.

PL-HA particles showed excellent toxicological profile without affecting the mitochondria in the macrophages for the tested period. We speculate that the HA coating may endow these nanotubes protection for a longer time inside the macrophages' cytoplasm since both CNT and CNT-PL-HA are well taken up by the macrophages (Fig. 6).

3.6. CNT-PL-HA do not induce a burst release of pro-inflammatory cytokines

Activation of the immune system by CNTs might cause toxic effects that could lead to tissue damage and cell death [34,35]. Two key cytokines were examined as markers for activation of the innate immune arm, the pro-inflammatory cytokine tumor necrosis factor (TNF)- α , and the anti-inflammatory cytokine interleukin 10 (IL-10). Their activity is counter-balanced by an anti-inflammatory response that prevents excessive damage to the host. TNF- α , the first cytokine to be released after activation, is mainly produced by monocytes and macrophages. It is regarded as the key pro-inflammatory cytokine [36,37]. TNF- α also induces the production of IL-10. IL-10 is produced

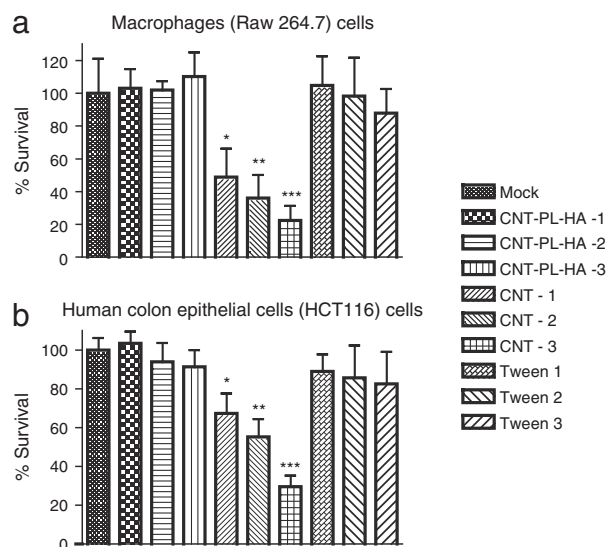


Fig. 5. CNT-PL-HA are not cytotoxic to macrophages and epithelial cells. The cytotoxic effect of CNT-PL-HA nanotubes on RAW (murine macrophages) and HCT (human epithelial) cell lines was examined using XTT proliferation assay. (a) Murine macrophages; (b) human colon epithelial cells treated and analyzed 72 h post incubation. Data are presented as mean \pm SD of 16–21 wells per treatment. CNT-PL-HA-, CNT-, and Tween-1,2,3 are representative concentrations of 4.8, 6.1 and 16.7 μ g/ml, respectively. *, **, *** denote $p < 0.05$, 0.01, and 0.001, respectively.

typically to inhibit activated macrophages by suppressing the production of TNF- α by macrophages [38]. To assess cytokine induction in response to the presence of CNT-PL-HA and several control nanotubes, an ELISA assay was established in the murine macrophage cell line.

Fig. 8a shows that no induction of IL-10 expression was observed at all nanotubes tested regardless of incubation time. TNF- α (Fig. 8b) was induced by CNT and by its solvent Tween 80. After 4 h of incubation, CNT induced TNF- α production at a level of almost 2-fold (23 ng/ml for the CNT compared with 13 ng/ml for Tween 80). After 24 h of incubation, CNT induced TNF- α at a level of almost four-fold to dramatic levels (42 ng/ml compared with 12 ng/ml of the Tween 80). As a control study, we also tested a free form of high molecular weight (HMw) HA and the conjugate (PL-HA) and did not observe production of IL-10 or TNF- α (data not shown). The data presented here strongly suggests that CNT and not its solvent (Tween 80) agonizes one of the innate immune receptors similar to LPS and may induce a robust pro-inflammatory response via Toll-like receptor (TLR)-4 or TLR2.

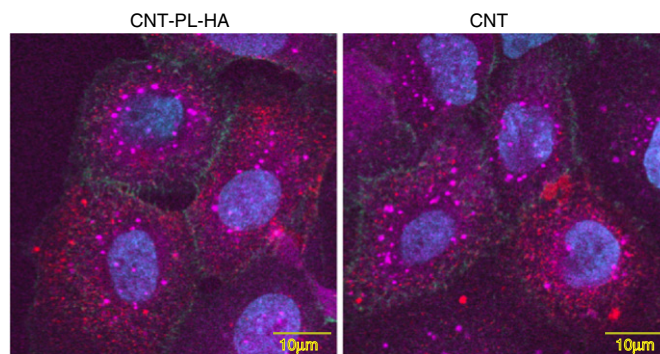


Fig. 6. CNT-PL-HA and CNT are taken up by macrophages. Representative confocal images demonstrating internalization of CNT- or CNT-PL-HA labeled with rhodamine into macrophages within 20 min of incubation. Nuclei staining (Hoechst), cell membrane boarders (Con A-AlexaF.488) and mitochondria staining (Deep Red labeled MitoTracker™).

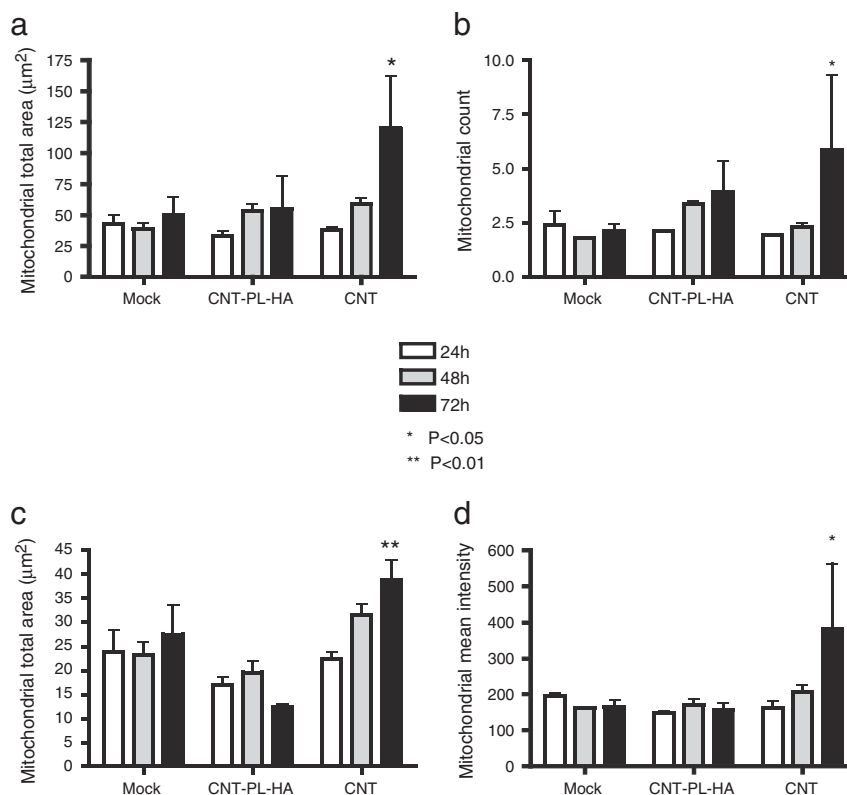


Fig. 7. No mitochondrial toxicity is observed when cells are treated with CNT-PL-HA. (a–d) Murine macrophages were cultured in the presence of 16.67 μg/ml of either CNT or CNT-PL-HA. Cells without CNTs served as control (Mock). Following 24, 48 or 72 h of culture, the cells were washed with PBS and after 8 h of recovery were stained with Hoechst 33342, Calcein AM, propidium iodide and Deep Red labeled MitoTracker. The stained cells were subjected to image acquisition employing the IN Cell Analyzer 2000 (GE Healthcare) and the obtained images were analyzed using the manufacturer's software to design a user-built algorithm for segmentation, linkage between different channels masks, measure set-up and sub-population classification. Several representative measures obtained from the analyses at the cell by cell level are depicted in bar graphs showing mean ± SEM of 4 independent wells per treatment; statistical analysis was done using a two way-ANOVA with Bonferroni post test analysis; * denotes $p < 0.05$; and ** denotes $p < 0.01$. HCA performed on murine macrophages revealed mitochondrial toxicity of CNTs but not of CNT-PL-HA, 72 h post culture.

We then moved to test the CNT-PL-HA upon systemic, and intravenous (i.v.) administration.

To gain additional insight into this immune activation by CNT, we also tested complement activation in human sera (Fig. 7c).

The complement system is an integral part of the innate immunity, where its inadvertent activation may induce clinically significant anaphylaxis [39]. Earlier we demonstrated that carbon nanotubes coated with human serum albumin, methoxyPEG₅₀₀₀-phospholipid, or covalently grafted to PEG of different chain lengths or covalently grafted to PEG and further coated with methoxyPEG₅₀₀₀-phospholipid can trigger complement activation in human serum [40–42]. Here we further show that nanotube surface coverage with HA-PL also fail to prevent complement activation. On the contrary, HA-PL coverage increased the level of the complement activation product SC5b-9 compared with the carboxylated surface. This phenomenon is highly interesting since HA-PL coating was shown previously to prevent complement activation by liposomes [26]. This increase in complement activation may be attributed to the initiation of complement activation through another pathway, but this was not investigated. Nevertheless, the gross architectural changes of immobilized HA on nanotube surfaces, when compared to liposomes, presumably allow sensing by certain complement initiating molecules such as ficolins and/or the highly cationic properdin [25]. These observations further highlight the difficulty in making the surface of carbon nanotubes inert with PEG and biopolymers to complement sensing, while conferring longevity to nanotubes in the systemic circulation.

3.7. CNT-PL-HA do not induce liver toxicity or alter the total number of leukocytes upon a single intravenous administration

To test the global liver toxicity (liver enzyme release and cholesterol levels) induced by CNT-PL-HA and pCNTs as well as any changes in the number of leukocytes or their differential profile, a single intravenous (i.v.) injection was performed into 8 week old C57BL/6 mice at a dose of 0.1 mg/ml ($n = 6$ mice/group). PBS treated mice served as control group, from which the basal levels of the AST, ALT and the cholesterol levels were taken. An additional group received the solvent, 1% Tween 80 in PBS. The results obtained with this group were at the same level of the basal level (data not shown). 2, 6 and 24 h post i.v. injections, blood was drawn from the retro-orbital sinus of each of the mice using a capillary tube. ALT, AST and serum cholesterol levels are shown in Fig. 9a–c.

The CNT treated groups showed a significant increase in AST and ALT enzyme serum levels already at 2 h post injection with substantial increase with time. No significant changes in liver enzyme levels were observed with the group treated with the CNT-PL-HA. In addition, there was no change in cholesterol level of neither of the tested groups indicating that the damage to the liver is transient and is not affecting metabolic parameters upon a single i.v. injection. It is already documented that coating lipid-based nanotubes with HA can stealth them from the immune system and that they do not accumulate in the liver and do not induce liver enzyme release [43,44]. In addition, the total number of leukocytes was not altered in the group

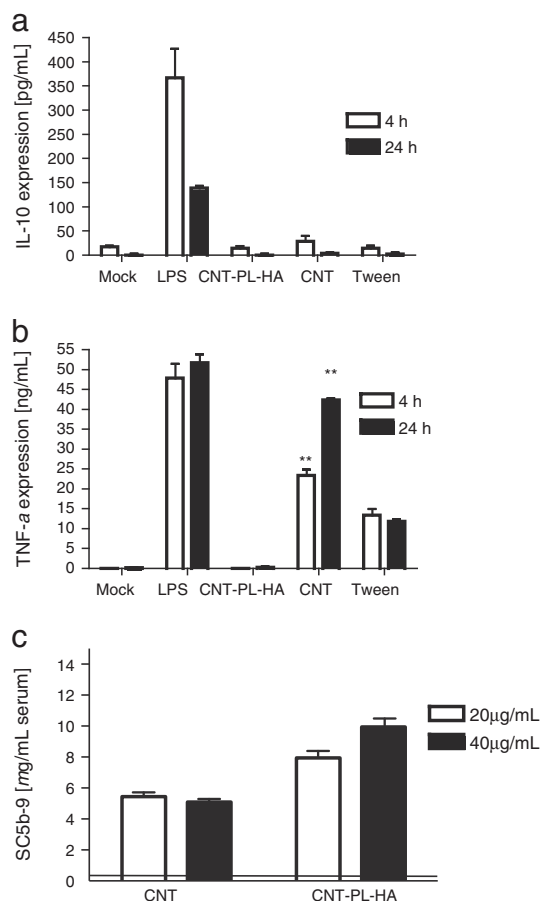


Fig. 8. CNT-PL-HA do not induce cytokine production. TNF- α and IL-10 induction measured by ELISA assay upon incubation with CNTs and CNT-PL-HA particles. (a) IL-10 production at 4 and 24 h post incubation with CNT and CNT-PL-HA particles. (b) same as in (a) but measuring the production of TNF- α . Data is presented as mean \pm SD of 16–21 wells per treatment. ** denotes $p < 0.01$. (c) CNT-mediated complement activation in a typical human serum. SC5b-9 is a non-lytic soluble marker of the terminal pathway of the complement system and a sensitive measure of the activation of the whole complement cascade. The horizontal lines indicate the baseline level of SC5b-9 in serum. Zymosan (1 mg/ml) was used as a positive control for complement activation, which generated $42.1 \pm 1.1 \mu\text{g}$ SC5b-9/ml.

treated with CNT-PL-HA and was comparable to the mock-treated group. In contrast, mice that were treated with CNTs had a substantial increase in the total number of leukocytes with an increase in the number of monocytes and a decrease in lymphocytes (Table 1).

3.8. CNT-PL-HA do not induce liver toxicity upon three intravenous administrations

We repeated the same experiment, but this time included 3 i.v. injections, as detailed in the experimental section, to examine the medium-term effect on the mice. We have not observed any dramatic changes in the results obtained upon multiple injections with the CNT-PL-HA supporting the hypothesis that PL-HA may provide a protective layer to the CNTs. However, when injecting pCNTs, 3 i.v. administrations have caused severe elevation in liver enzyme release (Fig. 10). In addition, 2 out of 5 mice experienced massive shivering 2 h post the 3rd injection, and we had to sacrifice the mice due to ethical reasons.

This immune activation often initiates when nanoparticles interact with cells of the innate immune arm such as monocytes, macrophages, and dendritic cells, in a similar manner to a pathogen infection or being sensed as a damaged tissue. This interaction may lead to signal cascades upon activation of pattern recognition

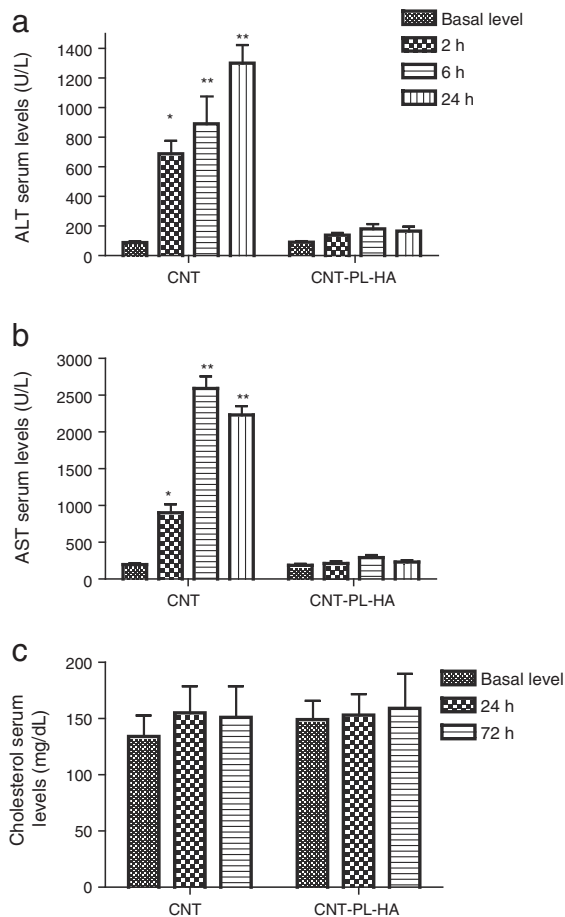


Fig. 9. CNT-PL-HA particles did not induce systemic toxicity upon single i.v. injection. Serum levels of liver enzymes Alanine Aminotransferase (ALT) (a) and Aspartate Aminotransferase (AST); (b) 2, 6 and 24 h post injection (c). Serum cholesterol level 24 h and 72 h post injection. All results refer to the administration of 100 μl of pristine CNTs or CNT-PL-HA particles at 0.1 mg/ml concentration in C57BL/6 mice. *, and ** denotes $p < 0.05$, and $p < 0.01$, respectively.

receptors (PRRs). PRRs are proteins expressed by cells of the innate immune arm to identify pathogen-associated molecular patterns (PAMPs), which are associated with microbial pathogens or cellular stress [34,45]. Thus, it is likely that the HA coating endows a

Table 1

Hematological parameters of mock-treated, CNT- and CNT-PL-HA treated mice.

	Normal ranges	Mock-treated	CNT-treated	CNT-PL-HA
PCV (%)	39–44	44 \pm 2	41 \pm 3	43 \pm 2
Hgb (g/dl)	10.2–16.6	13.4 \pm 2.1	14.7 \pm 3.4	13.9 \pm 1.5
WBC ($\times 1000$)	6–15	7.5 \pm 1.5	22 \pm 1**	9 \pm 1.0
<i>Diff. (%)</i>				
Lymphocytes	55–85	60 \pm 4.5	50 \pm 1.3**	59 \pm 5.2
Monocytes	1–4	3 \pm 0.5	25 \pm 1.1**	4 \pm 0.3
Eosinophils	0–4	2 \pm 0.1	0	3 \pm 0.1
Basophils	0–1	0	0	0
Plat ($\times 1000$)	160–410	200 \pm 50	120 \pm 38**	320 \pm 60

Results are the average \pm SEM of $n = 6$ mice/tested group.

PCV – packed cell volume – a measure of the proportion of blood volume that is occupied by red blood cells.

Hgb – hemoglobin levels.

WBC ($\times 1000/\text{ul}$) – white blood cell counts.

Diff. (%) – % of differentiated leukocytes.

Plat ($\times 1000$) – platelets – help control bleeding.

Bold data denote $p = 0.05$ or lower is considered statistically significant.

** Denotes $p < 0.001$.

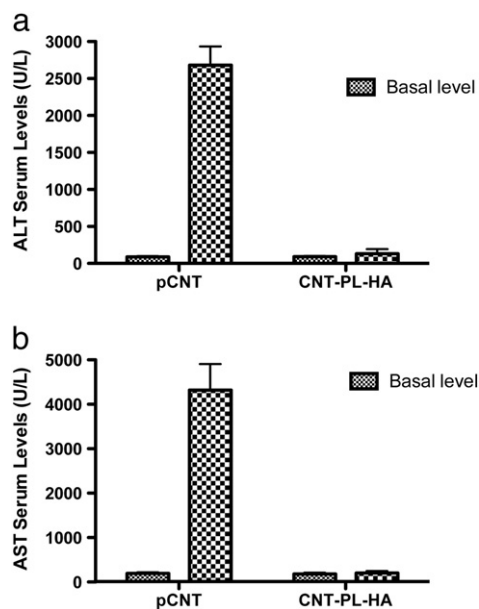


Fig. 10. CNT-PL-HA particles did not induce systemic toxicity upon multiple i.v. injections. Serum levels of liver enzymes Alanine Aminotransferase (ALT) (a) and Aspartate Aminotransferase (AST); (b), 24 h post the last i.v. injection. All results refer to the administration of 100 μ l of pristine CNTs or CNT-PL-HA particles at 0.1 mg/ml concentration in C57BL/6 mice.

protective layer from immune activation as we recently demonstrated for HA-coated liposomes [46].

The use of HA on the CNT surface may endow these carriers with long circulating and potentially tumor targeting capabilities to HA receptors, CD44 and CD168, that are highly expressed in tumor cells, as we and others previously demonstrated for other HA-coated nanovectors [30,43,47,48].

4. Conclusions

In this study, we have devised a new straightforward, inexpensive strategy to non-covalently functionalize pristine carbon nanotubes. The functionalization was facilitated with a biocompatible molecule, hyaluronan, which endows these particles with the potential to be applied in various biomedical applications. Once prepared, the new particles are easily dissolved and create stable aqueous solutions. No cytotoxicity was observed with macrophages or epithelial cells. In addition, incubating these particles with leukocytes did not induce pro-inflammatory cytokines or mitochondrial toxicity. Finally, no systemic toxicity was observed with CNT-PL-HA particles administered *in vivo* while pristine CNTs induced significant signs of toxicity such as altering the total numbers of lymphocytes and monocytes as well as releasing high levels of liver enzymes to the circulation, which are regarded as markers for liver toxicity. To apply these particles in variety of biological applications, other molecules can be loaded or bound to these particles, such as imaging agents, antibodies and small molecule drugs.

Taken together, the results presented here support the use of HA as a protective shield of CNTs from immune recognition and provide a protective layer against mitochondrial toxicity. The use of CNT-PL-HA may open new avenues for diagnostics and therapeutic modalities.

Acknowledgment

SMM acknowledges the financial support by the Danish Agency for Science, Technology and Innovation (Det Strategiske Forskningsråd),

reference 09-065746. PPW is a recipient of a Ph.D. scholarship award from the University of Copenhagen.

This work was supported in part by grants from the Lewis Family Trust, Israel Science Foundation (Award #181/10), the Israeli Centers of Research Excellence (I-CORE), Gene Regulation in Complex Human Disease, Center No 41/11, the FTA: Nanomedicine for Personalized Theranostics, and by The Leona M. and Harry B. Helmsley Nanotechnology Research Fund awarded to D.P.

References

- [1] F. Lu, L. Gu, M.J. Meziani, X. Wang, P.G. Luo, L.M. Veca, L. Cao, Y.-P. Sun, *Advances in bioapplications of carbon nanotubes*, *Adv. Mater.* 21 (2) (2009) 139–152.
- [2] In: R. Sirdeshmukh, K. Teker, B. Panchapakesan (Eds.), *Functionalization of Carbon Nanotubes with Antibodies for Breast Cancer Detection Applications*. MEMS, NANO and Smart Systems, 2004 ICMENS 2004 Proceedings 2004 International Conference on, Aug. 25–27 2004.
- [3] M. Prato, K. Kostarelos, A. Bianco, *Functionalized carbon nanotubes in drug design and discovery*, *Acc. Chem. Res.* 41 (1) (Jan 2008) 60–68, (PubMed PMID: 17867649).
- [4] T.K. Leeuw, R.M. Reith, R.A. Simonette, M.E. Harden, P. Cherukuri, D.A. Tsybouski, et al., *Single-walled carbon nanotubes in the intact organism: near-IR imaging and biocompatibility studies in *Drosophila**, *Nano Lett.* 7 (9) (Sep 2007) 2650–2654, (PubMed PMID: 17696559).
- [5] Y. Zhang, Y. Bai, B. Yan, *Functionalized carbon nanotubes for potential medicinal applications*, *Drug Discov. Today* 15 (11–12) (Jun 2010) 428–435, (PubMed PMID: 20451656).
- [6] D.A. Heller, S. Baik, T.E. Eurell, M.S. Strano, *Single-walled carbon nanotube spectroscopy in live cells: towards long-term labels and optical sensors*, *Adv. Mater.* 17 (23) (2005) 2793–2799.
- [7] Z. Liu, S.M. Tabakman, Z. Chen, H. Dai, *Preparation of carbon nanotube bioconjugates for biomedical applications*, *Nat. Protoc.* 4 (9) (2009) 1372–1382, (PubMed PMID: 19730421. Pubmed Central PMCID: 2853129).
- [8] Z. Liu, X. Sun, N. Nakayama-Ratchford, H. Dai, *Supramolecular chemistry on water-soluble carbon nanotubes for drug loading and delivery*, *ACS Nano* 1 (1) (Aug 2007) 50–56, (PubMed PMID: 19203129).
- [9] N.W. Kam, H. Dai, *Carbon nanotubes as intracellular protein transporters: generality and biological functionality*, *J. Am. Chem. Soc.* 127 (16) (Apr 27 2005) 6021–6026, (PubMed PMID: 15839702).
- [10] J. Cheng, K.A. Fernando, L.M. Veca, Y.P. Sun, A.I. Lamond, Y.W. Lam, et al., *Reversible accumulation of PEGylated single-walled carbon nanotubes in the mammalian nucleus*, *ACS Nano* 2 (10) (Oct 28 2008) 2085–2094, (PubMed PMID: 19206455).
- [11] Z. Liu, M. Winters, M. Holodniy, H. Dai, *siRNA delivery into human T cells and primary cells with carbon-nanotube transporters*, *Angew. Chem. Int. Ed. Engl.* 46 (12) (2007) 2023–2027, (PubMed PMID: 17290476).
- [12] M.S. Ladeira, V.A. Andrade, E.R. Gomes, C.J. Aguiar, E.R. Moraes, J.S. Soares, et al., *Highly efficient siRNA delivery system into human and murine cells using single-wall carbon nanotubes*, *Nanotechnology* 21 (38) (Sep 24 2010) 385101, (PubMed PMID: 20798464).
- [13] Z. Liu, K. Chen, C. Davis, S. Sherlock, Q. Cao, X. Chen, et al., *Drug delivery with carbon nanotubes for *in vivo* cancer treatment*, *Cancer Res.* 68 (16) (Aug 15 2008) 6652–6660, (PubMed PMID: 18701489. Pubmed Central PMCID: 2562710).
- [14] R. Crinelli, E. Carloni, M. Menotta, E. Giacomini, M. Bianchi, G. Ambrosi, et al., *Oxidized ultrashort nanotubes as carbon scaffolds for the construction of cell-penetrating NF- κ B decoy molecules*, *ACS Nano* 4 (5) (May 25 2010) 2791–2803, (PubMed PMID: 20411956).
- [15] M.R. McDevitt, D. Chattopadhyay, B.J. Kappel, J.S. Jaggi, S.R. Schifman, C. Antczak, et al., *Tumor targeting with antibody-functionalized, radiolabeled carbon nanotubes*, *J. Nucl. Med.* 48 (7) (Jul 2007) 1180–1189, (PubMed PMID: 17607040).
- [16] S.Y. Hong, G. Tobias, K.T. Al-Jamal, B. Ballesteros, H. Ali-Boucetta, S. Lozano-Perez, et al., *Filled and glycosylated carbon nanotubes for *in vivo* radioemitter localization and imaging*, *Nat. Mater.* 9 (6) (Jun 2010) 485–490, (PubMed PMID: 20473287).
- [17] Z. Liu, S. Tabakman, K. Welscher, H. Dai, *Carbon nanotubes in biology and medicine: *in vitro* and *in vivo* detection, imaging and drug delivery*, *Nano Res.* 2 (2) (Feb 1 2009) 85–120, (PubMed PMID: 20174481. Pubmed Central PMCID: 2824900).
- [18] M.S. Strano, *Probing chiral selective reactions using a revised Kataura plot for the interpretation of single-walled carbon nanotube spectroscopy*, *J. Am. Chem. Soc.* 125 (51) (2003) 16148–16153.
- [19] D. Peer, J.M. Karp, S. Hong, O.C. Farokhzad, R. Margalit, R. Langer, *Nanocarriers as an emerging platform for cancer therapy*, *Nat. Nanotechnol.* 2 (12) (Dec 2007) 751–760, (PubMed PMID: 18654426).
- [20] S. Mizrahy, D. Peer, *Polysaccharides as building blocks for nanotherapeutics*, *Chem. Soc. Rev.* 41 (7) (Apr 7 2012) 2623–2640, (PubMed PMID: 22085917).
- [21] D. Peer, E.J. Park, Y. Morishita, C.V. Carman, M. Shimaoka, *Systemic leukocyte-directed siRNA delivery revealing cyclin D1 as an anti-inflammatory target*, *Science* 319 (5863) (Feb 1 2008) 627–630, (PubMed PMID: 18239128. Pubmed Central PMCID: 2490797).
- [22] R. Kedmi, N. Ben-Arie, D. Peer, *The systemic toxicity of positively charged lipid nanoparticles and the role of Toll-like receptor 4 in immune activation*, *Biomaterials* 31 (26) (Sep 2010) 6867–6875, (PubMed PMID: 20541799).

- [23] S.S. Kim, D. Peer, P. Kumar, S. Subramanya, H. Wu, D. Asthana, et al., RNAi-mediated CCR5 silencing by LFA-1-targeted nanoparticles prevents HIV infection in BLT mice, *Mol. Ther.* 18 (2) (Feb 2010) 370–376, (PubMed PMID: 19997090).
- [24] X. Li, Y. Peng, J. Ren, X. Qu, Carboxyl-modified single-walled carbon nanotubes selectively induce human telomeric i-motif formation, *Proc. Natl. Acad. Sci. U. S. A.* 103 (52) (Dec 26 2006) 19658–19663, (PubMed PMID: 17167055. Pubmed Central PMCID: 1750900).
- [25] A.J. Andersen, J.T. Robinson, H. Dai, A.C. Hunter, T.L. Andresen, S.M. Moghimi, Single-walled carbon nanotube surface control of complement recognition and activation, *ACS Nano* 7 (2) (Jan 16 2013) 1108–1119, (PubMed PMID: 23301860).
- [26] S. Mizrahy, S.R. Raz, M. Hasgaard, H. Liu, N. Soffer-Tsur, K. Cohen, et al., Hyaluronan-coated nanoparticles: the influence of the molecular weight on CD44-hyaluronan interactions and on the immune response, *J. Control. Release* 156 (2) (Dec 10 2011) 231–238, (PubMed PMID: 21745506).
- [27] L.A. Mitchell, F.T. Lauer, S.W. Burchiel, J.D. McDonald, Mechanisms for how inhaled multiwalled carbon nanotubes suppress systemic immune function in mice, *Nat. Nanotechnol.* 4 (7) (Jul 2009) 451–456, (PubMed PMID: 19581899).
- [28] Z. Liu, S. Tabakman, K. Welsher, H.J. Dai, Carbon nanotubes in biology and medicine: *in vitro* and *in vivo* detection, imaging and drug delivery, *Nano Res.* 2 (2) (Feb 2009) 85–120, (PubMed PMID: ISI:000273939000001. English).
- [29] D.F. Williams, On the nature of biomaterials, *Biomaterials* 30 (30) (Oct 2009) 5897–5909, (PubMed PMID: 19651435).
- [30] I. Rivkin, K. Cohen, J. Koffler, D. Melikhov, D. Peer, R. Margalit, Paclitaxel-clusters coated with hyaluronan as selective tumor-targeted nanovectors, *Biomaterials* 31 (27) (Sep 2010) 7106–7114, (PubMed PMID: 20619792).
- [31] M. Cohen, Z. Kam, L. Addadi, B. Geiger, Dynamic study of the transition from hyaluronan- to integrin-mediated adhesion in chondrocytes, *EMBO J.* 25 (2) (Jan 25 2006) 302–311, (PubMed PMID: 16407968. Pubmed Central PMCID: 1383524).
- [32] D. Joester, E. Klein, B. Geiger, L. Addadi, Temperature-sensitive micrometer-thick layers of hyaluronan grafted on microspheres, *J. Am. Chem. Soc.* 128 (4) (Feb 1 2006) 1119–1124, (PubMed PMID: 16433527).
- [33] L.J. Solmesky, M. Shuman, M. Goldsmith, M. Weil, D. Peer, Assessing cellular toxicities in fibroblasts upon exposure to lipid-based nanoparticles: a high content analysis approach, *Nanotechnology* 22 (49) (Nov 21 2011) 494016, (PubMed PMID: 22101838).
- [34] D. Landesman-Milo, D. Peer, Altering the immune response with lipid-based nanoparticles, *J. Control. Release* 161 (2) (Jul 20 2012) 600–608, (PubMed PMID: 22230342).
- [35] D.F. Moyano, M. Goldsmith, D.J. Solfield, D. Landesman-Milo, O.R. Miranda, D. Peer, et al., Nanoparticle hydrophobicity dictates immune response, *J. Am. Chem. Soc.* 134 (9) (Mar 7 2012) 3965–3967, (PubMed PMID: 22339432. Pubmed Central PMCID: 3296893).
- [36] R. Ulevitch, Molecular mechanisms of innate immunity, *Immunol. Res.* 21 (2) (2000) 49–54.
- [37] B. Beutler, Inferences, questions and possibilities in Toll-like receptor signalling, *Nature* 430 (6996) (Jul 8 2004) 257–263, (PubMed PMID: 15241424).
- [38] C. Platzer, C. Meisel, K. Vogt, M. Platzer, H.D. Volk, Up-regulation of monocytic IL-10 by tumor necrosis factor- α and cAMP elevating drugs, *Int. Immunol.* 7 (4) (Apr 1995) 517–523, (PubMed PMID: 7547677).
- [39] S.M. Moghimi, P.P. Wibroe, S.Y. Helvig, Z.S. Farhangrazi, A.C. Hunter, Genomic perspectives in inter-individual adverse responses following nanomedicine administration: the way forward, *Adv. Drug Deliv. Rev.* 64 (13) (May 23 2012) 1385–1393, (PubMed PMID: 22634158).
- [40] A.J. Andersen, P.P. Wibroe, S.M. Moghimi, Perspectives on carbon nanotube-mediated adverse immune effects, *Adv. Drug Deliv. Rev.* 64 (15) (May 23 2012) 1700–1705, (PubMed PMID: 22634159).
- [41] S.M. Moghimi, A.J. Andersen, S.H. Hashemi, B. Lettiero, D. Ahmadvand, A.C. Hunter, et al., Complement activation cascade triggered by PEG-PL engineered nanomedicines and carbon nanotubes: the challenges ahead, *J. Control. Release* 146 (2) (Sep 1 2010) 175–181, (PubMed PMID: 20388529).
- [42] S.M. Moghimi, A.C. Hunter, Complement monitoring of carbon nanotubes, *Nat. Nanotechnol.* 5 (6) (Jun 2010) 382, (author reply –3. PubMed PMID: 20523330).
- [43] D. Peer, R. Margalit, Tumor-targeted hyaluronan nanoliposomes increase the antitumor activity of liposomal Doxorubicin in syngeneic and human xenograft mouse tumor models, *Neoplasia* 6 (4) (Jul-Aug 2004) 343–353, (PubMed PMID: 15256056. Pubmed Central PMCID: 1502115).
- [44] G. Bachar, K. Cohen, R. Hod, R. Feinmesser, A. Mizrahi, T. Shpitzer, et al., Hyaluronan-grafted particle clusters loaded with Mitomycin C as selective nanovectors for primary head and neck cancers, *Biomaterials* 32 (21) (Jul 2011) 4840–4848, (PubMed PMID: 21482433).
- [45] D. Peer, Immunotoxicity derived from manipulating leukocytes with lipid-based nanoparticles, *Adv. Drug Deliv. Rev.* 64 (15) (2012 Dec) 1738–1748, (PubMed PMID: 22820531).
- [46] D. Landesman-Milo, M. Goldsmith, S. Leviatan Ben-Arye, B. Witenberg, E. Brown, S. Leibovitch, et al., Hyaluronan grafted lipid-based nanoparticles as RNAi carriers for cancer cells, *Cancer Lett.* 334 (2) (Aug 27 2012) 221–227, (PubMed PMID: 22935680).
- [47] D. Peer, R. Margalit, Loading mitomycin C inside long circulating hyaluronan targeted nano-liposomes increases its antitumor activity in three mice tumor models, *Int. J. Cancer* 108 (5) (Feb 20 2004) 780–789, (PubMed PMID: 14696107).
- [48] R.E. Eliaz, F.C. Szoka Jr., Liposome-encapsulated doxorubicin targeted to CD44: a strategy to kill CD44-overexpressing tumor cells, *Cancer Res.* 61 (6) (Mar 15 2001) 2592–2601, (PubMed PMID: 11289136).